APPLICATION OF THE MULTIPLICATIVE-REGULARIZED GAUSS-NEWTON INVERSION FOR INVERTING 3D MARINE CSEM DATA

A. Abubakar, J. Liu, G. Pan, T. M. Habashy, M. Zaslavsky, V. Druskin, G. Cairns, C. Nalepa

Schlumberger, USA

1. INTRODUCTION

The marine controlled-source electromagnetic (CSEM) method has the potential of providing useful information in applications such as off-shore oil exploration. With a horizontal electric dipole as a transmitter towed by a ship and multi-component electromagnetic receivers on the seafloor, this method has been applied in several field surveys. The high contrast in resistivity between saline-filled rocks and hydrocarbons, makes this method well-suited for detecting oil reservoirs ([1, 2]). The approach initially employed is based on comparing the electric field amplitude as a function of the source-receiver offset with a similar measurement for a non-hydrocarbon-bearing reservoir, see [2]. The presence of hydrocarbon raises the amplitude of the measured electric field indicating the existence and, to some degree, determining the horizontal extent of the hydrocarbon zone. However, with this approach it is difficult to know the reservoir's depth and shape.

A more rigorous approach to address this type of application is the full nonlinear inversion approach (see [3, 4, 5]). In such an approach the investigation domain is subdivided into pixels and through inversion, the location, the shape and the conductivity of the reservoir are reconstructed. In this paper we applied the method developed in [5] for inverting three-dimensional (3D) field data. Unlike the methods in [3, 4], where the minimization approaches are based on non-linear conjugate gradient (CG) or quasi-Newton techniques, our method employed a Gauss-Newton minimization approach. The Gauss-Newton approach is known to have higher convergence rates than non-linear CG or quasi-Newton methods. The method is also equipped with the multiplicative regularization technique so that we do not need to determine the so-called regularization parameter in the optimization process. Further, the algorithm accomodates two different regularization schemes to produce either a smooth (using a standard L_2-norm function) or a blocky (using a weighted L_2-norm function) conductivity distribution ([6]). Moreover, to enhance the robustness of the algorithm, we incorporated a non-linear transformation for constraining the minimum and maximum values of the conductivity distribution. A line-search procedure for enforcing error reduction in the cost function in the minimization process is also employed. Since we are dealing with a large-scale computational problem, we will also touch upon an efficient parallel MPI (Message Passing Interface) implementation of our method.

2. THEORY

We consider a non-linear inverse problem described by the following equation: $\mathbf{d}^{\rm obs} = \mathbf{s}(\mathbf{m})$, where $\mathbf{d}^{\rm obs} = [d^{\rm obs}(\mathbf{r}_i^{\rm S}, \mathbf{r}_j^{\rm R}, \omega_k), i = 1, 2, \cdots, I; j = 1, 2, \cdots, J; k = 1, 2, \cdots, K]^T$ is the vector of measured data and $\mathbf{r}_i^{\rm S}$, $\mathbf{r}_j^{\rm R}$, and ω_k are the source position vector, the receiver position vector and the frequency of operation, respectively. The superscript ^{T} denotes the transpose of a vector. The vector $\mathbf{s}(\mathbf{m})$ represents simulated data computed by solving Maxwell equations:

$$\nabla \times \sigma^{-1}(\mathbf{r}) \nabla \times \mathbf{H}(\mathbf{r}) - {\rm i}\omega\mu \mathbf{H}(\mathbf{r}) = \nabla \times \sigma^{-1}(\mathbf{r}) \mathbf{J}(\mathbf{r}^{\rm S}) \,, \tag{1}$$

where $\nabla = (\partial_x, \partial_y, \partial_z)$ denotes the spatial differentiation operator, σ is the electrical conductivity, $\mathbf{r}$ is the spatial position, $\mathbf{H}$ is the magnetic field vector, $\mathrm{i}^2 = -1$, μ is a constant magnetic permeability, and $\mathbf{J}$ is the source vector. In the CSEM applications the source is an electric dipole oriented parallel to the tow line and the receiver can be any component of the magnetic or electric vector field. Equation (1) is discretized using the Lebedev grid employing a Dirichlet boundary condition at infinity. The computational domain is extended to infinity by using the optimal grid technique. The resulting linear system of equations (the stiffness matrix) is solved using a preconditioned quasi-minimum residual (QMR) iterative technique. The preconditioning operator is constructed by using an integral equation operator for layered background medium. The details of the forward algorithm can be found in [7].

The unknown vector model parameters are defined as: $\mathbf{m} = [m(x_l, y_t, z_q),\ l = 1, \cdots, L;\ t = 1, \cdots, T\ q = 1, \cdots, Q]$, where x_l, y_t and z_q denote the center of the discretization cell. We assume that there are $I \times J \times K$ number of data points in the survey and that the configuration can be described by $L \times T \times Q$ model parameters. The unknown model parameter $m(\mathbf{r}) = \sigma(\mathbf{r})/\sigma_0(\mathbf{r})$ is the normalized conductivity where $\sigma_0(\mathbf{r})$ is the conductivity distribution of the initial model used in the inversion.

Following [5], we pose the inverse problem as the minimization problem of a multiplicative cost function. Hence, at the n^{th} iteration, we reconstruct $\mathbf{m}_n$ that minimizes

$$\Phi_n(\mathbf{m}) = \phi^d(\mathbf{m}) \times \phi_n^m(\mathbf{m})\,, \tag{2}$$

where ϕ^d is the data misfit, given by:

$$\phi^d(\mathbf{m}) = \frac{1}{2}\sum_{k=1}^{K} \frac{\sum_{i=1}^{I}\sum_{j=1}^{J}\left|W_{d;i,j,k}\left[d_{i,j,k}^{\mathrm{obs}} - s_{i,j,k}(\mathbf{m})\right]\right|^2}{\sum_{i=1}^{I}\sum_{j=1}^{J}\left|W_{d;i,j,k}\, d_{i,j,k}^{\mathrm{obs}}\right|^2}\,, \tag{3}$$

in which $|\cdot|$ denotes the absolute value and $\boldsymbol{\mathcal{W}_d}$ is the data weighting matrix. The regularization function ϕ_n^m is given by,

$$\phi_n^m(\mathbf{m}) = \sum_{\kappa=x,y,z} \alpha_\kappa \int_D b_{\kappa;n}^2(x,y,z)\left\{\left|\partial_\kappa \ln\left[m(x,y,z)\right]\right|^2 + \delta_{\kappa;n}\right\}\mathrm{d}x\mathrm{d}y\mathrm{d}z\,,$$

where α_κ are the smoothing ratio factors and the weights $b_{\kappa;n}^2(x,y,z)$ are given by

$$b_{\kappa;n}^2(x,y,z) = \left[\int_D \left\{\left|\partial_\kappa \ln\left[m_n(x,y,z)\right]\right|^2 + \delta_{\kappa;n}\right\}\mathrm{d}x\mathrm{d}y\mathrm{d}z\right]^{-1} \tag{4}$$

for the L_2-norm regularizer and

$$b_{\kappa;n}^2(x,y,z) = \left[V\left\{\left|\partial_\kappa \ln\left[m_n(x,y,z)\right]\right|^2 + \delta_{\kappa;n}\right\}\right]^{-1}\,, \quad V = \int_D \mathrm{d}x\mathrm{d}y\mathrm{d}z \tag{5}$$

for the weighted L_2-norm regularizer as introduced in [6]. The L_2-norm regularizer is known to favor smooth profiles, while the weighted L_2-norm regularizer is known for its ability to preserve edges. The positive parameter $\delta_{\kappa;n}$ is a constant chosen to be: $\delta_{\kappa;n} = \phi^d(\mathbf{m}_n)/\left(\Delta\kappa\right)^2$, $\kappa = x, y, z$, where Δx, Δy and Δz are the widths of the discretization cell in the x, y, and z directions.

In the Gauss-Newton approach, at the n^{th} iteration, we obtain a set of linear equations for the search vector $\mathbf{p}_n$ (see [5]):

$$\boldsymbol{\mathcal{H}}_n \cdot \mathbf{p}_n = -\mathbf{g}_n\,, \tag{6}$$

where the approximate Gauss-Newton Hessian matrix is given by

$$\mathcal{H}_n \approx \mathcal{J}_n^T \cdot \mathcal{W}_d{}^T \cdot \mathcal{W}_d \cdot \mathcal{J}_n + \phi^d(\mathbf{m}_n)\, \mathcal{L}^{(2)}(\mathbf{m}_n)\,. \tag{7}$$

The matrix $\mathcal{J}_n$ is the Jacobian matrix and $\mathcal{L}^{(2)}(\mathbf{m}_n)$ is the second derivative of the regularization function in equation (4) with respect to $\mathbf{m}$ evaluated at $\mathbf{m} = \mathbf{m}_n$. The gradient of the cost function is given by

$$\mathbf{g}_n = -\mathcal{J}_n^T \cdot \mathcal{W}_d{}^T \cdot \mathcal{W}_d \cdot \left[\mathbf{d}^{\text{obs}} - \mathbf{s}(\mathbf{m}_n)\right] + \phi^d(\mathbf{m}_n)\, \mathcal{L}^{(1)}(\mathbf{m}_n) \cdot \mathbf{m}_n\,, \tag{8}$$

where $\mathcal{L}^{(1)}(\mathbf{m}_n)\cdot\mathbf{m}_n$ is the first derivative of the regularization function in equation (4) with respect to $\mathbf{m}$ evaluated at $\mathbf{m} = \mathbf{m}_n$.

This multiplicative cost function will apply a large weight on the regularization factor at the beginning of the optimization process because the value of $\phi^d(\mathbf{m})$ is still large. In this case, the search direction is predominantly a steepest descent, which is more appropriate to use in the initial steps of the iteration process because it has the tendency to suppress large swings in the search direction. As the iteration proceeds, the optimization process will gradually reduce the error in the data misfit while the regularization factor $\phi_n^m(\mathbf{m})$ remains at a nearly constant value close to unity. In this case, the search direction corresponds to a Newton search direction, which is more appropriate to use as we get closer to the minimum of the data misfit cost function $\phi^d(\mathbf{m})$ where the quadratic model of the cost function becomes more accurate. If noise is present in the data, the data misfit cost function $\phi^d(\mathbf{m})$ will plateau to a certain value determined by the signal-to-noise ratio; in which case, the weight, λ_n, on the regularization factor will be non-zero. In this way, the noise will, at all times, be suppressed in the inversion process and the need for a larger regularization will be automatically imposed when the data contain noise.

After the Gauss-Newton search vector $\mathbf{p}_n$ is obtained, solving the linear system of equations in equation (6) using a conjugate gradient least-square (CGLS) technique, the unknown model parameters are updated using a non-linear transformation and a line-search procedure. More details on the algorithm can be found in [5].

3. FIELD DATA INVERSION

We present inversion results of the data set collected in offshore west of Africa. This data set is collected using 11 tow-lines and 66 receivers as shown in figure 1. The data contains 8 frequencies: 0.0625, 0.1875, 0.25, 0.3125, 0.4375, 0.75, 1.25, and 1.75 Hz.

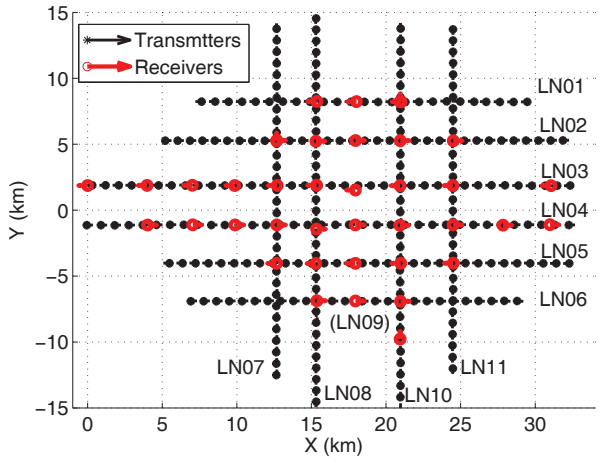

Fig. 1. The deep water survey region and tow-lines.

The survey covers a region of 35 km by 35 km. However, due to the limitation of our computational resources, we only inverted data from two parallel tow-lines (LN03 and LN04). Further we only used in-line data (the electric field components in the tow-direction (the x-direction) due to electric dipole sources that are oriented in the x-direction). Hence, we only have 20 receiver stations (10 in each tow-line). In each tow-line, the receivers are located along 34 km line. We inverted data at a single-frequency at 0.25 Hz with 30 sources per tow-line. In total, we only have 178 complex-valued data points (some of the sources did not use all receivers available).

The seawater depth varies between 1.3 and 1.7 km in the y-direction across these two tow-lines and it is nearly flat in the x-direction. The inversion domain is 34 km by

20 km by 6 km and divided into 170 by 100 by 120 grids with a cell size of 200 m by 200 m by 50 m. As a starting model we employed a model consisting of an air layer, several water layers and a homogeneous sea-bottom with conductivity 0.43 S/m. We stopped the inversion after fifteen iterations when the values of the data misfit did not significantly decrease any further. In figure 2 we show the inversion results in the xy-plane at the expected reservior depth and in the xz-planes where LN03 and LN04 tow-lines are located. In these figures the colorbars are given in terms of the resistivity and we have intentionally hidden

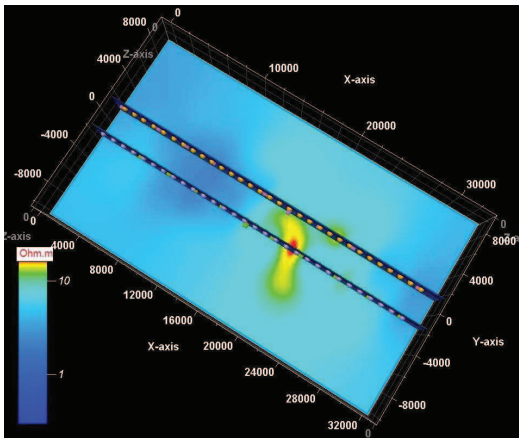

(a) xy-plane at the expected reservior depth.

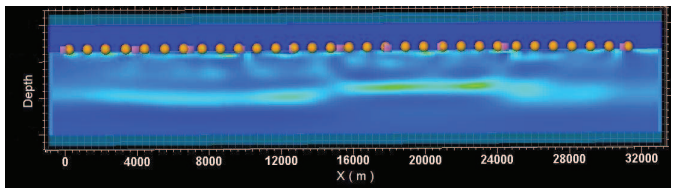

(b) xz-plane at $y = 1.4$ km (over the tow-line LN03)

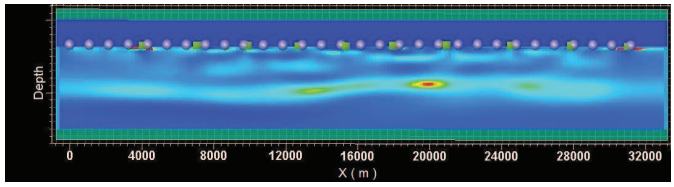

(c) xz-plane at $y = -1.6$ km (over the tow-line LN04)

Fig. 2. Inversion results.

the depth axis because of the data confidentiality issue. From the inversion results we observe the presence of the reservoir at a depth that is agreed with the resistivity measurements in an exploration well in the area. The resistivity value of the reservoir is close to 15 ohm.m. In the presentation we will also show inversion results from data containing more than two tow-lines.

4. REFERENCES

[1] S. C. Constable, C. S. Cox, and A. D. Chave, "Offshore electromagnetic surveying techniques," in *SEG Expanded Abstracts*, pp. 81–82. SEG Expanded Abstracts, 1986.

[2] T. Eidesmo, S. Ellingsrud, L. M. MacGregor, S. Constable, M. C. Sinha, S. Johansen, F. N. Kong, and H. Westerdahl, "Sea bed logging (SBL), a new method for remote and direct identification of hydrocarbon filled layers in deepwater areas," *First Break*, vol. 20, no. 3, pp. 144–152, 2002.

[3] R. E. Plessix and W. A. Mulder, "Resistivity imaging with controlled-source electromagnetic data: depth and data weighting," *Inverse Problems*, vol. 24, pp. 1–21, 2008.

[4] M. Commer and G. Newman, "New advances in three-dimensional controlled source electromagnetic inversion," *Geophysical Journal International*, vol. 172, pp. 513–535, 2008.

[5] A. Abubakar, T. Habashy, V. Druskin, L. Knizhnerman, and D. Alumbaugh, "2.5d forward and inverse modeling for interpreting low-frequency electromagnetic measurements," *Geophysics*, vol. 73, no. 4, pp. F165–F177, July-August 2008.

[6] P. M. van den Berg and A. Abubakar, "Constrast source inversion method: State of art," *Progress in Electromagnetic Research*, vol. 34, pp. 189–218, 2001.

[7] M. Zaslavsky, S. Davydycheva, V. Druskin, L. Knizherman, A. Abubakar, and T. Habashy, "Finite-difference solution of the three-dimensional electromagnetic problem using divergence free preconditioners," in *SEG Expanded Abstracts*, vol. 25, pp. 775–778. 2006.